International Journal of Bifurcation and Chaos

Electronic version of an article published as
International Journal of Bifurcation and Chaos, Vol.27, No.7 (2017) 1750101 (16 pages)

DOI: 10.1142/S0218127417501012

PERIOD DOUBLING BIFURCATION POINT DETECTION STRATEGY WITH NESTED LAYER PARTICLE SWARM OPTIMIZATION

HARUNA MATSUSHITA
Dept. of Electronics and Information Engineering, Kagawa University
2217-20 Hayashi-cho, Takamatsu, Kagawa 761-0396, Japan
haruna@eng.kagawa-u.ac.jp

YUSHO TOMIMURA
**Dept. of Mechanical and Energy Systems Engineering, Oita University*
700 Dannoharu, Oita 870–1192, Japan

HIROAKI KUROKAWA
Dept. of Electric and Electronic Engineering, Tokyo University of Technology
1404-1 Katakuramachi, Hachioji City, Tokyo 192–0982, Japan
hkuro@cs.teu.ac.jp

TAKUJI KOUSAKA*
takuji@oita-u.ac.jp

Received (to be inserted by publisher)

This paper proposes a bifurcation point detection strategy based on nested layer particle swarm optimization (NLPSO). The NLPSO is performed by two particle swarm optimization (PSO) algorithms with a nesting structure. The proposed method is tested in detection experiments of period doubling bifurcation points in discrete-time dynamical systems. The proposed method directly detected the parameters of period doubling bifurcation regardless of the stability of the periodic point, but require no careful initialization, exact calculation or Lyapunov exponents. Moreover, the proposed method is an effective detection technique in terms of accuracy, robustness usability, and convergence speed.

Keywords: bifurcation point detection, bifurcation analysis, initial value setup problem, discrete-time dynamical systems, particle swarm optimization (PSO)

1. Introduction

Many real-world systems including engineering, biological, social and ecological systems can be modeled as dynamical systems with one or more parameters. As the parameters are varied, the periodic solutions of the system may undergo a sudden qualitative change called a *bifurcation*. Bifurcation analysis is among the most important nonlinear analysis techniques for understanding phenomena of systems.

Bifurcation parameters can be detected or traced by various methods [Kawakami, 1984; Ueta *et al.*, 1997; Kousaka *et al.*, 1999]. Moreover, many software packages have been developed for bifurcation analysis, such as AUTO [Doedel & Oldeman, 2012] and BunKi [ERATO, JST, 2004]. However, these conventional

methods are based on the Newton–Raphson method, which is a gradient-based algorithm. Therefore, they require derivation of the system equations and appropriate initial values.

Alternatively, bifurcation analysis can be performed by population-based optimization (also called swarm intelligence), a metaheuristic optimization that offers multiple potential solutions. A particularly popular algorithm is Particle Swarm Optimization (PSO) [Kennedy & Eberhart, 1995], which does not derivate the objective functions. Despite its simplicity, PSO performs global search and has many real/potential applications. Barrera et al. [Barrera *et al.*, 2008] proposed an application of PSO for plotting bifurcation diagrams in the analysis of dynamical systems. This method finds all stable/unstable equilibrium points for a parameter by using PSO. Although this method generates a bifurcation diagram by finely changing the parameter and plotting all equilibrium points for each value of the parameter, it cannot directly detect the bifurcation parameters from the parameter space of the system. On the other hand, Matsushita et al. proposed a PSO-based method that directly detects period doubling bifurcation parameters in switched dynamical systems [Matsushita & Saito, 2011]. Although this method is low-dimensional and requires no carefully set initial system parameters, it detects the bifurcation parameter by exactly deriving the unstable periodic point, which involves a complicated calculation. In other words, this method cannot be applied to the system which the periodic point cannot be exactly derived such as a circle map described below.

Therefore, this method lacks versatility. Meanwhile, PSO-based periodic point detection methods [Parsopoulos & Vrahatis, 2003; Skokos *et al.*, 2005; Liu *et al.*, 2006; Petalas *et al.*, 2008; Gao *et al.*, 2009] quickly and accurately find the periodic points without a Lyapunov or gradient-based method although these methods cannot detect the bifurcation parameters.

This paper proposes a nested layer particle swarm optimization (NLPSO) for directly detecting period doubling bifurcation points. The NLPSO is performed by two nested PSOs. The inner PSO processes a single agent in the main PSO. Although two objective functions in NLPSO influence each other, they are not optimized simultaneously. In bifurcation point detection, the main PSO searches for the period doubling bifurcation parameters, whereas the inner PSO searches for the periodic point using the system parameter, which corresponds to the information of one agent in the main PSO. Using the periodic point returned by the inner PSO, the main PSO calculates the objective function for that agent under the bifurcation conditions. The initial value problem of conventional bifurcation analyses can then be solved by applying the NLPSO-detected bifurcation point to the initial point of the bifurcation curve tracing.

We apply our bifurcation point detection method to three discrete-time dynamical systems; a circle map, a Hénon map [Hénon, 1976] and coupled Hénon maps [Sausedo-Solorio & Pisarchik, 2011]. In these experiments, the proposed method accurately detected the period doubling bifurcation parameters directly from the parameter space, regardless of the stability of the periodic point. Moreover, the proposed method requires no carefully set initial values or exact calculations.

The rest of the paper is organized as follows. Section 2 explains definitions of a discrete-time dynamical system and its bifurcation of fixed and periodic points. Section 3 mentions an algorithm of the PSO. Section 4 proposes a novel approach, NLPSO, to detect bifurcation parameters of unstable/stable fixed and periodic points, by using two nested PSOs. Section 5 illustrates the validity and applicability of the NLPSO through several examples. Section 6 shows comparison results with the bifurcation point detection method by using the single PSO, and evaluates the effectiveness of the proposed approach which is two nested PSOs. Finally, Section 7 concludes our works and states several directions of research found in our agenda.

2. Definition

Let us consider an N-dimensional discrete-time dynamical system described by

$$\boldsymbol{x}_{k+1} = \boldsymbol{f}(\boldsymbol{x}_k, \boldsymbol{\lambda}), \tag{1}$$

where k denotes the discrete time, and $\boldsymbol{x}_k \in \mathbb{R}^N$ and $\boldsymbol{\lambda} \in \mathbb{R}^L$ correspond to the state variables and system parameters, respectively.

Let $\boldsymbol{f}^l$ denote the l-th iteration of $\boldsymbol{f}$. A point $\boldsymbol{x}_p \in \mathbb{R}^N$ is said to be an n-periodic point of $\boldsymbol{f}$ if $\boldsymbol{x}_p$ satisfies $\boldsymbol{x}_p = \boldsymbol{f}^n(\boldsymbol{x}_p, \boldsymbol{\lambda})$ and $\boldsymbol{x}_p \neq \boldsymbol{f}^l(\boldsymbol{x}_p, \boldsymbol{\lambda})$ for $l < n$. A 1-periodic point is referred to as a fixed point.

The Jacobian matrix of $\boldsymbol{f}^n$ is described by

$$D\boldsymbol{f}^n(\boldsymbol{x}_p, \boldsymbol{\lambda}) = \prod_{l=0}^{p-1} \frac{\partial \boldsymbol{f}}{\partial \boldsymbol{x}_l}(\boldsymbol{x}_l, \boldsymbol{\lambda}), \tag{2}$$

with characteristic equation

$$\det\left(D\boldsymbol{f}^n(\boldsymbol{x}_p, \boldsymbol{\lambda}) - \mu \boldsymbol{I}_N\right) = 0, \tag{3}$$

where $\boldsymbol{I}_N$ denotes the $N \times N$ identity matrix, and μ is a characteristic multiplier of $D\boldsymbol{f}^n(\boldsymbol{x}_p, \boldsymbol{\lambda})$. The characteristic multipliers determine the local stability class of an n-periodic point. If all characteristic multipliers of $D\boldsymbol{f}^n(\boldsymbol{x}_p, \boldsymbol{\lambda})$ are inside the unit circle in the complex plane, then $\boldsymbol{x}_p$ is a stable periodic point (SPP). If any characteristic multipliers of $D\boldsymbol{f}^n(\boldsymbol{x}_p, \boldsymbol{\lambda})$ are outside the unit circle, then $\boldsymbol{x}_p$ is an unstable periodic point (UPP).

When $\mu = -1$, the period doubling bifurcates at periodic points $\boldsymbol{x}_p$. Thus, the bifurcation condition is given by

$$\det\left(D\boldsymbol{f}^n(\boldsymbol{x}_p, \boldsymbol{\lambda}) + \boldsymbol{I}_N\right) = 0. \tag{4}$$

3. Particle Swarm Optimization (PSO)

The PSO is a population-based evolutionary computation technique that gives multiple potential solutions, called *particles*. Each particle carries position and velocity information. The position vector of the i-th particle at iteration t and its velocity vector are represented by $\boldsymbol{z}_i(t) = (z_{i1}, z_{i2}, \cdots, z_{iD}) \in \mathbb{R}^D$ and $\boldsymbol{v}_i(t) = (v_{i1}, v_{i2}, \cdots, v_{iD}) \in \mathbb{R}^D$, respectively, where $(i = 1, 2, \cdots, M)$, M is the number of particles in the swarm and D corresponds to the dimension of a solution space. The position vector corresponds to an objective variable of the optimization. Each particle moves toward its personal best position $\boldsymbol{p}_i = (p_{i1}, p_{i2}, \cdots, p_{iD})$ (*pbest*), which defines its best previous position, and the global best position $\boldsymbol{p}_g = (p_{g1}, p_{g2}, \cdots, p_{gD})$ (*gbest*) defining the best *pbest* with the best objective value among all particles. Therefore, $\boldsymbol{p}_g$ is the global optimum solution at iteration t. The d^{th} dimension element of $\boldsymbol{v}_i$ and $\boldsymbol{z}_i$ on each particle i are updated according to [Shi & Eberhart, 1998]

$$\begin{aligned} v_{id}(t+1) &= w v_{id} + r_1 c_1 (p_{id} - z_{id}(t)) + r_2 c_2 (p_{g_d} - z_{id}(t)), \\ z_{id}(t+1) &= z_{id}(t) + v_{id}(t+1), \end{aligned} \tag{5}$$

where $(d = 1, 2, \cdots, D)$. The w is an inertia weight determining how much of the particle's previous velocity is preserved. The c_1 and c_2 are two fixed positive acceleration coefficients; usually $c_1 = c_2$. In this study, these three parameters are set to their optimal default values [Trelea, 2003], namely, $w = 0.729$ and $c_1 = c_2 = 1.494$. The r_1 and r_2 are two uniform random numbers taking different values between 0 and 1 at each dimension d. Algorithm 1 is the pseudo code of the PSO that minimizes the optimization, where $T_{\max}$ is the maximum iteration, C is the stop criterion, and g is an index of a particle whose *pbest* has the smallest objective value among all particles.

4. Bifurcation Point Detection Strategy with Nested Layer Particle Swarm Optimization (NLPSO)

We now propose the NLPSO and apply it to the detection of period doubling bifurcation points. PSO is among the simplest and most popular of the population-based optimization algorithms, so it was selected for the present study.

The NLPSO-based strategy for detecting period doubling bifurcation points is here described in detail. The proposed method finds the system parameters $\boldsymbol{\lambda}$ that produces a period doubling bifurcation of an n-periodic point in a dynamical system $\boldsymbol{f}$. The parameter $\boldsymbol{\lambda}$ is searched by two PSOs with a nested structure. The main PSO, called "PSO_{bif}", seeks the bifurcation parameter $\boldsymbol{\lambda}$. Thus, an objective variable $\boldsymbol{z_b}$ corresponding to the position vector of the PSO_{bif} is given by $\boldsymbol{z_b} \equiv \boldsymbol{\lambda} \equiv (\lambda_1, \lambda_2, \cdots, \lambda_L)$, and the objective function $F_{\text{bif}}(\boldsymbol{z_b})$ of the PSO_{bif} is defined as

$$F_{\text{bif}}(\boldsymbol{z_b}) = \left|\det\left(D\boldsymbol{f}^n(\boldsymbol{x}_p, \boldsymbol{z_b}) - \mu \boldsymbol{I}_N\right)\right|. \tag{6}$$

Algorithm 1 Pseudo code of the PSO.

▷ *Objective variable* $\boldsymbol{z}$
▷ *Objective function* $F(\boldsymbol{z})$.
Randomly initialize the position $\boldsymbol{z}$ of each particle i by uniformly distributing the particles over the search space $[z_{\min}, z_{\max}]^D$.
Initialize other particle variables as $\boldsymbol{v}_i(0) = 0$, $\boldsymbol{p}_i = \boldsymbol{z}_i(0)$ and $\boldsymbol{p}_g = \boldsymbol{z}_1(0)$.
Iteration counter $t \leftarrow 0$.
while ($t < T_{\max}$ OR $F(\boldsymbol{p}_g) > C$) **do**
  $t \leftarrow t + 1$
  for $i = 1$ to M, all M particles **do**
    Calculate $F(\boldsymbol{z}_i(t))$.
    if $F(\boldsymbol{z}_i(t)) < F(\boldsymbol{p}_i)$ **then**
      Update *pbest* of particle i as $\boldsymbol{p}_i = \boldsymbol{z}_i(t)$.
    end if
  end for i
  Update *gbest* $\boldsymbol{p}_g$, where $g = \arg\min_i F(\boldsymbol{p}_i)$.
  for $i = 1$ to M, all M particles **do**
    for $d = 1$ to D, all D dimensions **do**
      Update v_{id} and z_{id} according to Eq. (5).
    end for d
  end for i
end while
Output the final results $\boldsymbol{p}_g$.

Equation (6) defines the bifurcation condition at the n-periodic point $\boldsymbol{x}_p$ according to Eq. (3), where $F_{\text{bif}}(\boldsymbol{z_b}) = 0$ means that $\boldsymbol{z_b}$ produces a period doubling bifurcation at $\boldsymbol{x}_p$ when $\mu = -1$. Thus, it is a minimization optimization problem with a minimum at 0.

In Eq. (6), the n-periodic point $\boldsymbol{x}_p$ obviously depends on the system parameter $\boldsymbol{z_b} \equiv \boldsymbol{\lambda}$. In other words, we must derive M_{bif} periodic points given by the information of the respective M_{bif} particles in the PSO_{bif}. In the proposed method, these are searched by an inner PSO called "PSO_{pp}". A position vector of the PSO_{pp} is assigned a corresponding variable $\boldsymbol{z_p} \equiv \boldsymbol{x}_p \equiv (x_{p1}, x_{p2}, \cdots, x_{pN})$, and an objective function of the PSO_{pp} is defined as

$$F_{\text{pp}}(\boldsymbol{z_p}) = \|\boldsymbol{f}^n(\boldsymbol{z_p}, \boldsymbol{\lambda}) - \boldsymbol{z_p}\|, \tag{7}$$

where $\|\cdot\|$ denotes Euclidean distance, and $\boldsymbol{f}^n(\boldsymbol{z_p}, \boldsymbol{\lambda})$ corresponds to the state variable which is the n-th iteration of $\boldsymbol{f}$ with the initial point $\boldsymbol{z_p}$ and the parameter $\boldsymbol{\lambda}$, as described in Eq. (1). $F_{\text{pp}}(\boldsymbol{z_p}) = 0$ means that $\boldsymbol{z_p}$ is an n-periodic point of the map $\boldsymbol{f}$.

Algorithm 2 is the pseudo code of PSO_{bif}, namely our proposed NLPSO, and Algorithm 3 is the pseudo code of PSO_{pp}, which is called by PSO_{bif}. L and N correspond to the number of system parameters and the number of state variables in the dynamical system, M_{bif} and M_{pp} are the number of particles in the PSO_{bif} and PSO_{pp}, $T_{\max 1}$ and $T_{\max 2}$ are the maximum iterations on the PSO_{bif} and PSO_{pp}, C_{bif} and C_{pp} are the stop criteria of the PSO_{bif} and PSO_{pp}, and $\boldsymbol{p}_{\boldsymbol{p}_i}$ and $\boldsymbol{p}_{\boldsymbol{p}_g}$ are the *pbest* of the particle i and the *gbest* in the PSO_{pp}, respectively. The most important feature of the NLPSO is its detection of the bifurcation parameter and periodic point by the nested PSOs, not by solving a multi-objective problem. In other words, the PSO_{pp} is fully included in the PSO_{bif}. For each particle in the PSO_{bif}, a periodic point is detected by the PSO_{pp} every time the objective variables of the PSO_{bif} are updated. Therefore, the proposed method accurately solves two interdependent objective functions. Furthermore, as the NLPSO is based on PSO, it requires neither the Lyapunov exponent nor the second-order differential of the map (c.f. the Newton–Raphson method). Thus, rather than carefully specifying the initial values, we need only distribute them randomly through the search spaces of the two PSOs.

Algorithm 2 Pseudo code of bifurcation point detection strategy by the NLPSO.

▷ *Objective variable* $\boldsymbol{z_b}$ *corresponding to bifurcation parameter* $\boldsymbol{\lambda}$ *on the map* $\boldsymbol{f}$.
▷ *Objective function* $F_{\mathrm{bif}}(\boldsymbol{z_b})$.
Initialize particle information of the $\mathrm{PSO_{bif}}$.
Iteration counter $t_1 \leftarrow 0$.
while ($t_1 < T_{\max 1}$ OR $F_{\mathrm{bif}}(\boldsymbol{p}_g) > C_{\mathrm{bif}}$) **do**
  $t_1 \leftarrow t_1 + 1$
  for $i = 1$ to M_{bif}, all M_{bif} particles **do**
    $\boldsymbol{x}_p \leftarrow$ **PSOPP**$(\boldsymbol{z_{b}}_i(t_1))$ ▷ *Carry out the* PSO_{pp} *in Algorithm 3.*
    Evaluate $F_{\mathrm{bif}}(\boldsymbol{z_{b}}_i(t_1))$ with $\boldsymbol{x}_p$.
    Update *pbest* $\boldsymbol{p}_i$ if $F_{\mathrm{bif}}(\boldsymbol{z_{b}}_i(t_1)) < F_{\mathrm{bif}}(\boldsymbol{p}_i)$.
  end for i
  Update *gbest* $\boldsymbol{p}_g$, where $g = \arg\min_i F_{\mathrm{bif}}(\boldsymbol{p}_i)$.
  for $i = 1$ to M_{bif}, all M_{bif} particles **do**
    for $d = 1$ to L, all L dimensions **do**
      Update v_{bid} and z_{bid} according to Eq. (5).
    end for d
  end for i
end while
Output the final results $\boldsymbol{p}_g$ as a bifurcation parameter $\boldsymbol{\lambda}$.

Algorithm 3 Pseudo code of $\mathrm{PSO_{pp}}$ that finds n-periodic point.

procedure PSOPP$(\boldsymbol{\lambda})$
  ▷ *Objective variable* $\boldsymbol{z_p}$ *corresponding to n-periodic point* $\boldsymbol{x}_p$.
  ▷ *Objective function* $F_{\mathrm{pp}}(\boldsymbol{z_p})$.
  Initialize particle information of the $\mathrm{PSO_{pp}}$.
  Iteration counter $t_2 \leftarrow 0$.
  while ($t_2 < T_{\max 2}$ OR $F_{\mathrm{pp}}(\boldsymbol{p}_{\boldsymbol{p}_g}) > C_{\mathrm{pp}}$) **do**
    $t_2 \leftarrow t_2 + 1$
    for $i = 1$ to M_{pp}, all M_{pp} particles **do**
      Evaluate $F_{\mathrm{pp}}(\boldsymbol{z}_{\boldsymbol{p}_i}(t_2))$ with $\boldsymbol{\lambda}$.
      Update *pbest* $\boldsymbol{p}_{\boldsymbol{p}_i}$ if $F_{\mathrm{pp}}(\boldsymbol{z}_{\boldsymbol{p}_i}(t_2)) < F_{\mathrm{pp}}(\boldsymbol{p}_{\boldsymbol{p}_i})$.
    end for i
    Update *gbest* $\boldsymbol{p}_{\boldsymbol{p}_g}$, where $g = \arg\min_i F_{\mathrm{pp}}(\boldsymbol{p}_{\boldsymbol{p}_i})$.
    for $i = 1$ to M_{pp}, all M_{pp} particles **do**
      for $d = 1$ to N, all N dimensions **do**
        Update $v_{p_{id}}$ and $z_{p_{id}}$ according to Eq. (5).
      end for d
    end for i
  end while
  return $\boldsymbol{p}_{\boldsymbol{p}_g}$ ▷ *The n-periodic point depending on* $\boldsymbol{\lambda}$ *is* $\boldsymbol{p}_{\boldsymbol{p}_g}$.
end procedure

5. Simulations

In this section, the proposed bifurcation point detection strategy is applied to three discrete-time dynamical systems; the circle map, the Hénon map and the coupled Hénon maps.

Table 1. Variables and parameters of the nested PSOs in NLPSO.

	$\mathrm{PSO_{bif}}$	$\mathrm{PSO_{pp}}$
Objective variable $\boldsymbol{z}$	$\boldsymbol{z_b} \equiv \boldsymbol{\lambda}$	$\boldsymbol{z_p} \equiv \boldsymbol{x}_p$
Number of dimensions D	L	N
Stop criterion C	1×10^{-3}	1×10^{-5}
Maximum iterations $T_{\max}$	300	
Number of particles M	30	
Inertia weight w	0.729	
Acceleration coefficients c_1, c_2	1.494	

Table 2. Values of the initialization range for variables on the circle map.

Variable	λ_1 $(= z_{b1})$	λ_2 $(= z_{b2})$	x_p $(= z_{p1})$
Range	$[0.4, 0.6]$	$[0.5, 2]$	$[0, 1]$

5.1. *Circle map*

The circle map is a one-dimensional map described by

$$x_{k+1} = \left(x_k + \lambda_1 - \frac{\lambda_2}{2\pi} \sin 2\pi x_k \right) \mod 1.0, \tag{8}$$

where x is a state variable, and $\boldsymbol{\lambda} = (\lambda_1, \lambda_2)$ are system parameters. The circle map exhibits bifurcation phenomena as these parameters are varied.

From Eq. (8), the objective function of the $\mathrm{PSO_{bif}}$, which detects the period doubling bifurcation parameters, is defined as

$$\begin{aligned} F_{\mathrm{bif}}(\boldsymbol{z_b}) &= \left| \frac{dx_{p+n}}{dx_p} + 1 \right|, \\ &= \left| \prod_{l=1}^{n} (1 - z_{b2} \cos 2\pi x)|_{x=x_{n-l}} + 1 \right|, \end{aligned} \tag{9}$$

where $\boldsymbol{z_b} \equiv (z_{b1}, z_{b2}) \equiv \boldsymbol{\lambda} \equiv (\lambda_1, \lambda_2)$; thus, $L = 2$.

The objective function of the $\mathrm{PSO_{pp}}$, which detects an n-periodic point depending on the parameter set (λ_1, λ_2) corresponding to the particle information of the $\mathrm{PSO_{bif}}$, is defined as

$$F_{\mathrm{pp}}(\boldsymbol{z_p}) = |x_{p+n} - x_p|, \tag{10}$$

where $\boldsymbol{z_p} \equiv z_{p1} \equiv x_p$; thus, $N = 1$.

Table 1 summarizes the experimental parameters of $\mathrm{PSO_{bif}}$ and $\mathrm{PSO_{pp}}$. The position vectors of the $\mathrm{PSO_{bif}}$ and $\mathrm{PSO_{pp}}$ are randomly initialized by uniformly distributing the particles over the search space summarized in Table 2.

Implementing the NLPSO, we detected the period doubling bifurcation point in a circle map with n = 1-, 2-, 3- and 4-periodic points. These four kinds of periodic points can be handled by the same algorithm and objective functions, and require only a change of the parameter n. For each periodic point, we ran 10 simulations with different random initial states. The evaluation results of the 10 simulations are summarized in Table 3. Here we show the bifurcation parameters (λ_1, λ_2), the accuracy F_{bif}, the iteration count t_{end} at which F_{bif} satisfies the stop criterion 10^{-3}, the (λ_1, λ_2)-dependent periodic point x_p and its accuracy F_{pp} and the stability of x_p. On $n = 1$, no obtained parameter set satisfied an accuracy 10^{-3}. This means that there is no period doubling bifurcation of the fixed point in the search area set in Table 2. Thus, we can know whether there is the bifurcation of a certain periodic point, from the results of the proposed method. We should note that the proposed method automatically searches and detects bifurcation parameters that exist outside the initialization range, if the search area is not fixed and the period doubling bifurcation of the fixed point exists on the map. On the other hand, in $n = 2$,

Table 3. Ten parameters for detecting period doubling bifurcations of 1-, 2-, 3- and 4-periodic points in the circle map by NLPSO.

n	$\mathrm{PSO_{bif}}$				$\mathrm{PSO_{pp}}$		
	λ_1	λ_2	F_{bif}	t_{end}	x_p	F_{pp}	Stability
1	0.5775	1.9399	2.0000	300	0.7500	1.1375×10^{-1}	-
	0.5662	1.8005	2.0000	300	0.7500	1.4721×10^{-1}	-
	0.5264	1.8276	2.0000	300	0.7500	1.8269×10^{-1}	-
	0.5532	1.8285	2.0000	300	0.7500	1.5579×10^{-1}	-
	0.5721	1.8156	2.0000	300	0.7500	1.3892×10^{-1}	-
	0.5213	1.9865	2.0000	300	0.7500	1.6253×10^{-1}	-
	0.5726	1.8053	2.0000	300	0.7500	1.4006×10^{-1}	-
	0.5322	1.9879	2.0000	300	0.7500	1.5143×10^{-1}	-
	0.5143	1.7907	2.0000	300	0.7500	2.0073×10^{-1}	-
	0.5431	1.8282	2.0000	300	0.7500	1.6589×10^{-1}	-
2	0.4849	1.4303	9.823×10^{-4}	18	0.4957	3.063×10^{-6}	UPP
	0.4772	1.4494	4.208×10^{-4}	40	0.4938	1.711×10^{-6}	SPP
	0.4354	1.6603	2.379×10^{-4}	25	0.4888	6.224×10^{-6}	SPP
	0.5800	1.7667	6.790×10^{-4}	15	0.1099	0.672×10^{-6}	UPP
	0.5834	1.7912	7.469×10^{-4}	15	0.5106	7.043×10^{-6}	SPP
	0.5264	1.4617	9.557×10^{-4}	2	0.5070	8.873×10^{-6}	UPP
	0.5449	1.5429	6.180×10^{-4}	2	0.0706	6.727×10^{-6}	SPP
	0.5451	1.5443	2.646×10^{-4}	20	0.5101	0.413×10^{-6}	UPP
	0.5316	1.4804	9.969×10^{-4}	12	0.5081	4.599×10^{-6}	SPP
	0.4387	1.6391	6.625×10^{-4}	12	0.9092	1.204×10^{-6}	SPP
3	0.4187	1.6398	3.3374×10^{-4}	73	0.5779	5.0088×10^{-6}	UPP
	0.5574	1.8390	9.8542×10^{-4}	30	0.8603	6.1523×10^{-6}	SPP
	0.5839	1.6178	0.6322×10^{-4}	17	0.6396	2.7895×10^{-6}	SPP
	0.5870	1.5922	7.4816×10^{-4}	64	0.6393	9.6834×10^{-6}	UPP
	0.5948	1.5283	5.7181×10^{-4}	5	0.6386	3.4706×10^{-6}	SPP
	0.4524	1.9195	3.4548×10^{-4}	22	0.3558	1.7976×10^{-6}	SPP
	0.5952	1.5248	1.6775×10^{-4}	60	0.4194	9.7486×10^{-6}	UPP
	0.4513	1.9105	7.4865×10^{-4}	59	0.1454	4.7055×10^{-6}	UPP
	0.4057	1.5321	2.7524×10^{-4}	16	0.5805	9.6616×10^{-6}	SPP
	0.4159	1.6166	3.3157×10^{-4}	15	0.3605	7.9602×10^{-6}	UPP
4	0.4490	1.7017	4.4905×10^{-4}	12	0.5159	4.5465×10^{-6}	UPP
	0.5052	1.7709	9.6108×10^{-4}	31	0.2231	3.6549×10^{-6}	SPP
	0.5310	1.6395	7.3691×10^{-4}	30	0.9613	2.6709×10^{-6}	UPP
	0.5256	1.6349	4.3558×10^{-4}	11	0.5585	3.7924×10^{-6}	UPP
	0.5323	1.6417	6.6667×10^{-4}	28	0.1744	0.7098×10^{-6}	UPP
	0.4769	1.6357	6.3260×10^{-4}	40	0.0625	4.8761×10^{-6}	UPP
	0.5136	1.6676	8.1362×10^{-4}	58	0.9026	4.9990×10^{-6}	UPP
	0.5114	1.6857	1.7137×10^{-4}	28	0.8937	4.4500×10^{-6}	UPP
	0.5042	1.7885	5.4865×10^{-4}	32	0.4500	8.2079×10^{-6}	SPP
	0.4793	1.6385	9.6333×10^{-4}	57	0.5348	7.1889×10^{-6}	SPP

3- and 4-periodic points, the proposed method obtained the bifurcation parameters to an accuracy of 10^{-3}, regardless of the periodic number or the stability of the periodic point. We can obtain 2-dimensional bifurcation diagram by plotting the 2 bifurcation parameters, (λ_1, λ_2), obtained by the proposed method. Furthermore, we ran 50 simulations with different initial states, and the results are shown in Table 4. The table shows the mean $F_{\mathrm{bif}}(\boldsymbol{p}_g)$ and $F_{\mathrm{pp}}(\boldsymbol{p}_g)$, and their standard deviations (SD), and the mean t_{end} on the $\mathrm{PSO_{bif}}$. In the table, Suc[%] on the $\mathrm{PSO_{bif}}$ and the $\mathrm{PSO_{pp}}$ denote the success rate in achieving $F_{\mathrm{bif}}(\boldsymbol{p}_g) < C_{\mathrm{bif}}$ and $F_{\mathrm{pp}}(\boldsymbol{p}_g) < C_{\mathrm{pp}}$, respectively. We can confirm that the success rate of the $\mathrm{PSO_{bif}}$ is 100%, and the mean t_{end} is well below the iteration limit $T_{\mathrm{max1}} = 300$ on the $\mathrm{PSO_{bif}}$. In addition, the success rate of the $\mathrm{PSO_{pp}}$ is also 100%. Since the standard deviation values of both F_{bif} and F_{pp} are low, the proposed method has high robustness.

Table 4. Simulation results on the circle map over 50 independent trials.

n	$\mathrm{PSO_{bif}}$				$\mathrm{PSO_{pp}}$		
	Mean F_{bif}	SD F_{bif}	Mean t_{end}	Suc[%]	Mean F_{pp}	SD F_{pp}	Suc[%]
2	5.03×10^{-4}	2.79×10^{-4}	21.58	100	4.73×10^{-6}	2.75×10^{-6}	100
3	4.53×10^{-4}	2.45×10^{-4}	40.14	100	4.74×10^{-6}	3.21×10^{-6}	100
4	5.05×10^{-4}	2.81×10^{-4}	32.20	100	4.97×10^{-6}	3.06×10^{-6}	100

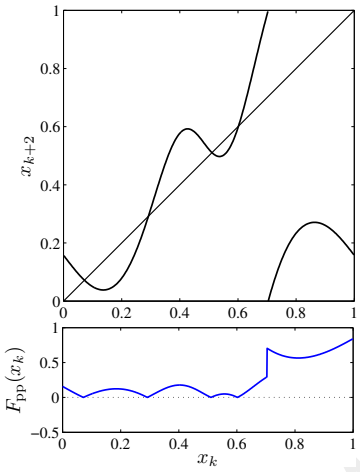

Fig. 1. Return map of the circle map onto the x_k–x_{k+2} plane (top) and the value of the objective function $F_{\mathrm{pp}}(x_k)$ (bottom) for the parameter set $(\lambda_1, \lambda_2) = (0.5449, 1.529)$ and the number of periodic points $n = 2$.

Let us consider the behavior of the $\mathrm{PSO_{pp}}$. Since the particle position z_{p_1} of the $\mathrm{PSO_{pp}}$ corresponds to x_k in the circle map described in Eq. (8), the particles move on a return map onto the x_k–x_{k+2} plane in the case of $n = 2$. The return map onto the x_k–x_{k+2} plane and the values of the objective function F_{pp} for the parameter set $\boldsymbol{z_b} \equiv (\lambda_1, \lambda_2) = (0.5449, 1.529)$ are shown in Fig. 1. If $x_k = x_{k+2} = f^2(x_k, \boldsymbol{\lambda})$, x_k is a 2-periodic point x_p. Two 2-periodic points (a UPP and an SPP) coexist in the map with this parameter set, namely, $(x_k, x_{k+1}, x_{k+2}) = (0.07175, 0.51062, 0.07175)$ (SPP) and $(x_k, x_{k+1}, x_{k+2}) = (0.29184, 0.60175, 0.29184)$ (UPP). Both of two 2-periodic points are optimal solutions, and their objective function values $F_{\mathrm{pp}}(x_k)$ take 0 which is the minimum value, as shown in the figure. Since the purpose of the $\mathrm{PSO_{pp}}$ is to find x_p satisfying $F_{\mathrm{pp}}(x_p) < C_{\mathrm{pp}}(= 10^{-5})$, the particles converge to either the UPP or the SPP depending on the initial state and the random number values in the update equation (Eq. (5)). Generally speaking, we should note that it is harder to find the UPP than finding the SPP. Figure 2 shows the movement of the $\mathrm{PSO_{pp}}$ particles converging to the SPP. The circles in this figure denote the position vectors $\boldsymbol{z_p}(\equiv x_p)$ of 30 particles in the $\mathrm{PSO_{pp}}$. In the initial state (a), the particles were randomly spread throughout the search space. As the iterations proceeded, the particles swarmed toward one of the two 2-periodic points (b). At $t_2 = 48$ (c), the $\mathrm{PSO_{pp}}$ found a stable 2-periodic point satisfying the criterion $F_{\mathrm{pp}} < 10^{-5}$, and terminated the periodic point searching. Panel (d) shows the result of running the maximum number of iterations without terminating the search at (c). Clearly, the swarm converged to the found SPP. Figure 3 shows the behavior of the swarm converging to a UPP. Identically to the SPP, the $\mathrm{PSO_{pp}}$ found the UPP at $t_2 = 27$ (c). These results confirm that $\mathrm{PSO_{pp}}$ accurately can find both SPPs and UPPs within a small number of iterations without careful initialization.

Now suppose that a $\mathrm{PSO_{bif}}$ particle takes parameters for which no 2-periodic point exists. Figure 4 shows the return map and values of the objective function $F_{\mathrm{pp}}(x_p)$ for $(\lambda_1, \lambda_2) = (0.41, 1.41)$ and $n = 2$. Under the conditions of this parameter set, there is no 2-periodic point satisfying $F_{\mathrm{pp}}(x_p) = 0$. Therefore, the $\mathrm{PSO_{pp}}$ cannot find a 2-periodic point even after the maximum number of simulations ($t_2 = 300$). Instead, the particles converge to a *false periodic point* that most closely approximates $F_{\mathrm{pp}}(x_p) = 0$ but lies outside the criterion 10^{-5}. Moreover, the false periodic point yields bad $F_{\mathrm{bif}}(\boldsymbol{z_b})$ values. For example, in the case of this parameter set, the $\mathrm{PSO_{pp}}$ converges to the false periodic point $x_f = 0.4613$ whose

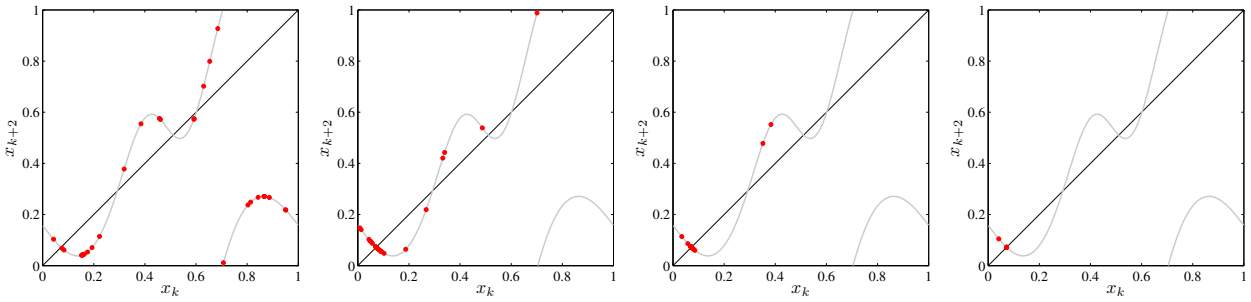

(a) $t_2 = 0$ (b) $t_2 = 15$ (c) $t_2 = 48$ (d) $t_2 = 300$

Fig. 2. Movement of the $\mathrm{PSO_{pp}}$ particles that converge to a stable periodic point. $\boldsymbol{z_b} \equiv (\lambda_1, \lambda_2) = (0.5449, 1.529)$ and $n = 2$.

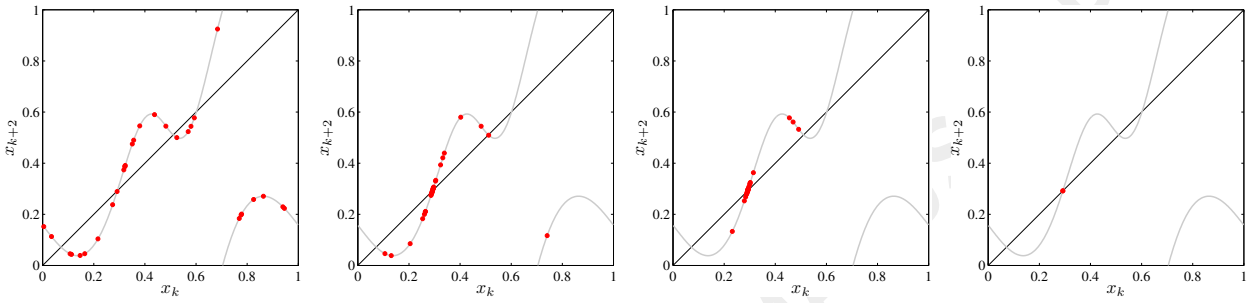

(a) $t_2 = 0$ (b) $t_2 = 15$ (c) $t_2 = 27$ (d) $t_2 = 300$

Fig. 3. Movement of the $\mathrm{PSO_{pp}}$ particles that converge to an unstable periodic point. $\boldsymbol{z_b} \equiv (\lambda_1, \lambda_2) = (0.5449, 1.529)$ and $n = 2$.

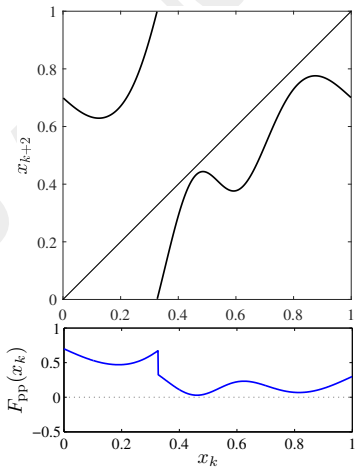

Fig. 4. Return map of the circle map onto x_k–x_{k+2} plane (top) and the objective function value $F_{\mathrm{pp}}(x_k)$ (bottom) for $(\lambda_1, \lambda_2) = (0.41, 1.41)$ and $n = 2$.

$F_{\mathrm{pp}}(x_f) = 0.0294$ that most closely approximates 0 but is larger than 10^{-5}. The value of F_{bif} depending on the x_f takes 1.9986 which is bad value. Therefore, when a $\mathrm{PSO_{bif}}$ particle takes the parameters for which no n-periodic point exists, it becomes attracted to particles with good F_{bif} values (parameters for which n-periodic points exist) through the PSO behavior. As the iterations proceed, the $\mathrm{PSO_{bif}}$ swarm automatically converges to the parameter area containing the n-periodic points, without requiring special manipulation or careful initialization.

From these results, we conclude that the proposed method effectively detects period doubling bifurcation points with high accuracy, high robustness, versatile usability and rapid convergence speed.

Table 5. Values of the initialization range for variables on the Hénon map.

Variable	λ_1 $(= z_{b1})$	λ_2 $(= z_{b2})$	(x_p, y_p) $(= \boldsymbol{z}_p)$
Range	$[1.44, 1.55]$	$[0.08, 0.28]$	$[-2, 2]^N$

5.2. *Hénon map*

Next, we consider the Hénon map, a two-dimensional map described by

$$\begin{aligned} x_{k+1} &= 1 - \lambda_1 x_k^2 + y_k, \\ y_{k+1} &= \lambda_2 x_k, \end{aligned} \tag{11}$$

where x and y are state variables. This map is governed by two parameters, λ_1 and λ_2, and exhibits chaotic behavior.

By definition of the Hénon map, the objective function of the $\mathrm{PSO_{bif}}$, which detects the period doubling bifurcation parameter, is defined as

$$\begin{aligned} F_{\mathrm{bif}}(\boldsymbol{z_b}) &= \left| \det \left(\frac{\partial \boldsymbol{f}^n}{\partial \boldsymbol{x}_p}(\boldsymbol{x}_p, \boldsymbol{z_b}) + \boldsymbol{I} \right) \right|, \\ &= \left| \det \left(\prod_{l=1}^{n} \left[\begin{array}{cc} -2z_{b1}x & 1 \\ z_{b2} & 0 \end{array} \right] \Bigg|_{x=x_{n-l}, y=y_{n-l}} + \left[\begin{array}{cc} 1 & 0 \\ 0 & 1 \end{array} \right] \right) \right|, \end{aligned} \tag{12}$$

where $\boldsymbol{z_b} \equiv (z_{b1}, z_{b2}) \equiv \boldsymbol{\lambda} \equiv (\lambda_1, \lambda_2)$; thus, $L = 2$ and $\boldsymbol{x}_p \equiv (x_p, y_p)$.

The objective function of the $\mathrm{PSO_{pp}}$ detects n-periodic points depending on the parameter set (λ_1, λ_2) corresponding to the particle information of the $\mathrm{PSO_{bif}}$, and is defined by

$$\begin{aligned} F_{\mathrm{pp}}(\boldsymbol{z_p}) &= \left\| \boldsymbol{f}^n(\boldsymbol{x}_p, \boldsymbol{\lambda}) - \boldsymbol{x}_p \right\|, \\ &= \sqrt{(x_{p+n} - x_p)^2 + (y_{p+n} - y_p)^2}, \end{aligned} \tag{13}$$

where $\boldsymbol{z_p} \equiv (z_{p1}, z_{p2}) \equiv \boldsymbol{x}_p \equiv (x_p, y_p)$, thus $N = 2$.

The experimental parameters of $\mathrm{PSO_{bif}}$ and $\mathrm{PSO_{pp}}$ are same as Table 1. The initialization ranges of the search space are summarized in Table 5.

To show that the proposed NLPSO-based method also detects bifurcations of high-periodic points, we investigated the period doubling bifurcation in the Hénon map with $n = 5$- and 10-periodic points. Existence of these period doubling bifurcations within the range of Table 5 was shown in [Gallas, 1993]. The results of 10 simulations are summarized in Table 6. The proposed method effectively detected the bifurcation parameter (λ_1, λ_2) in all cases. Furthermore, all of the detected bifurcation points satisfied the criterion $F_{\mathrm{bif}} < 10^{-3}$ in fewer iterations than the maximum number of iterations. The $\mathrm{PSO_{pp}}$ found both 5- and 10-periodic points to high accuracy without requiring careful initialization, gradient information or a Lyapunov exponent. Table 7 shows simulation results on the Hénon map over 50 independent trials. As with the case of the circle map, the success rates of both the $\mathrm{PSO_{bif}}$ and $\mathrm{PSO_{pp}}$ are 100%, and the mean t_{end} of the $\mathrm{PSO_{bif}}$ is well below the iteration limit $T_{\mathrm{max1}} = 300$. In addition, the standard deviation values of two PSOs are low.

5.3. *Two unidirectionally coupled Hénon maps*

To evaluate the performance of the proposed method for higher dimensional map including three or more system parameters, we consider coupled Hénon maps described by

$$\begin{aligned} x_{1k+1} &= 1 - \lambda_1 x_{1k}^2 + y_{1k}, \\ y_{1k+1} &= -\lambda_2 x_{1k}, \\ x_{2k+1} &= 1 - \lambda_1 x_{2k}^2 + y_{2k} + \lambda_3 \left(y_{1k} - y_{2k} \right), \\ y_{2k+1} &= -\lambda_2 x_{2k}, \end{aligned} \tag{14}$$

Table 6. Period doubling bifurcation parameters of Hénon map obtained by NLPSO.

n	PSO_{bif}				PSO_{pp}		
	λ_1	λ_2	F_{bif}	t_{end}	x_p	y_p	F_{pp}
5	1.4793	0.1449	3.7138×10^{-4}	18	-0.0872	0.1251	0.6077×10^{-6}
	1.4634	0.1877	4.0075×10^{-4}	21	0.0150	0.1528	2.7439×10^{-6}
	1.5146	0.1495	2.5196×10^{-4}	29	-0.1354	0.1299	0.7533×10^{-6}
	1.4831	0.1254	1.3124×10^{-4}	15	-0.8070	0.1381	1.7815×10^{-6}
	1.4773	0.1420	9.1392×10^{-4}	15	-0.8407	0.1580	8.9383×10^{-6}
	1.5079	0.0975	9.6671×10^{-4}	52	0.8425	0.0230	7.6945×10^{-6}
	1.4587	0.1913	4.7892×10^{-4}	18	0.8128	-0.0134	7.8566×10^{-6}
	1.5044	0.1494	2.3750×10^{-4}	41	1.1064	-0.0185	8.2760×10^{-6}
	1.4507	0.2032	9.1908×10^{-4}	22	0.0499	0.1635	9.1023×10^{-6}
	1.4777	0.2597	5.7330×10^{-4}	44	-0.9474	0.3012	4.8925×10^{-6}
10	1.4996	0.1113	8.5539×10^{-4}	61	0.1833	-0.0880	9.2084×10^{-6}
	1.5193	0.1646	2.4472×10^{-4}	19	0.7853	-0.0321	9.2233×10^{-6}
	1.4643	0.1947	8.5373×10^{-4}	44	-0.9667	0.2259	9.5778×10^{-6}
	1.4901	0.1362	7.3279×10^{-4}	39	-0.0106	0.1137	8.0206×10^{-6}
	1.5043	0.1059	6.3880×10^{-4}	66	-0.7811	0.1151	2.5365×10^{-6}
	1.4661	0.1931	0.5779×10^{-4}	101	1.1590	0.0021	2.0733×10^{-6}
	1.4885	0.1318	7.6538×10^{-4}	108	0.1996	-0.1050	2.7535×10^{-6}
	1.5077	0.1714	2.0962×10^{-4}	44	-0.9595	0.1948	1.8605×10^{-6}
	1.5330	0.1468	6.5261×10^{-4}	45	-0.0193	-0.1289	6.9358×10^{-6}
	1.4650	0.2404	8.9497×10^{-4}	64	0.7613	-0.0174	9.3318×10^{-6}

Table 7. Simulation results on the Hénon map over 50 independent trials.

n	PSO_{bif}				PSO_{pp}		
	Mean F_{bif}	SD F_{bif}	Mean t_{end}	Suc[%]	Mean F_{pp}	SD F_{pp}	Suc[%]
5	4.52×10^{-4}	2.93×10^{-4}	25.76	100	7.09×10^{-6}	2.30×10^{-6}	100
10	5.43×10^{-4}	2.84×10^{-4}	43.50	100	6.97×10^{-6}	4.31×10^{-6}	100

where x_1, y_1, x_2 and y_2 are state variables, and λ_1, λ_2 and λ_3 are parameters. The map is composed of two Hénon maps unidirectionally coupled via variable y_2, thus, $\lambda_3 \in [0, 1]$ is the coupling strength. Therefore, the two coupled Hénon maps is a four-dimensional map including three parameters.

By definition of the two coupled Hénon maps, the objective function of the PSO_{bif}, which detects the period doubling bifurcation parameter, is defined as

$$
\begin{aligned}
F_{\text{bif}}(\boldsymbol{z_b}) &= \left| \det \left(\frac{\partial \boldsymbol{f}^n}{\partial \boldsymbol{x}_p}(\boldsymbol{x}_p, \boldsymbol{z_b}) + \boldsymbol{I} \right) \right|, \\
&= \left| \det \left(\prod_{l=1}^{n} \begin{bmatrix} -2z_{b1}x_1 & 1 & 0 & 0 \\ -z_{b2} & 0 & 0 & 0 \\ 0 & z_{b3} & -2z_{b1}x_2 & 1-z_{b3} \\ 0 & 0 & -z_{b2} & 0 \end{bmatrix} \right|_{x_1=x_{1n-l}, y_1=y_{1n-l}, x_2=x_{2n-l}, y_2=y_{2n-l}} \right. \\
&\qquad \left. + \begin{bmatrix} 1 & 0 & 0 & 0 \\ 0 & 1 & 0 & 0 \\ 0 & 0 & 1 & 0 \\ 0 & 0 & 0 & 1 \end{bmatrix} \right) \Bigg|,
\end{aligned}
\tag{15}
$$

where $\boldsymbol{z_b} \equiv (z_{b1}, z_{b2}, z_{b3}) \equiv \boldsymbol{\lambda} \equiv (\lambda_1, \lambda_2, \lambda_3)$; thus, $L = 3$ and $\boldsymbol{x}_p \equiv (x_{1p}, y_{1p}, x_{2p}, y_{2p})$.

The objective function of the PSO_{pp} detects n-periodic points depending on the parameter set

Table 8. Values of the search range for variables on the two coupled Hénon maps.

Variable	λ_1 $(= z_{b1})$	λ_2 $(= z_{b2})$	λ_3 $(= z_{b3})$	$(x_{1p}, y_{1p}, x_{2p}, y_{2p})$ $(= \boldsymbol{z}_p)$
Range	$[1.44, 1.55]$	$[0.08, 0.28]$	$[0, 1]$	$[-2, 2]^N$

Table 9. Period doubling bifurcation parameters of the two coupled Hénon maps obtained by NLPSO.

n	$\mathrm{PSO_{bif}}$					$\mathrm{PSO_{pp}}$				
	λ_1	λ_2	λ_3	F_{bif}	t_{end}	x_{1p}	y_{1p}	x_{2p}	y_{2p}	F_{pp}
4	1.3109	0.1161	0.9431	2.9625×10^{-4}	174	-0.04239	-0.10380	0.99293	-0.00814	8.8834×10^{-6}
	1.4425	0.0958	0.3821	5.4293×10^{-4}	24	-0.21828	-0.08808	0.94555	-0.00687	8.7415×10^{-6}
	1.3875	0.1459	0.6311	8.2389×10^{-4}	16	0.87028	0.00649	-0.34518	-0.13908	8.8899×10^{-6}
	1.4068	0.1780	0.6119	4.9500×10^{-4}	3	0.84877	0.00203	0.08125	-0.13830	8.8609×10^{-6}
	1.3761	0.1375	0.6631	1.4698×10^{-5}	89	-0.04948	-0.12049	0.79036	0.04830	9.6838×10^{-6}
	1.3948	0.0999	0.5369	1.8740×10^{-4}	71	0.89488	0.01061	-0.33958	-0.09596	8.9445×10^{-6}
	1.3886	0.1243	0.5992	4.7588×10^{-4}	56	0.88284	0.00910	-0.34354	-0.11904	9.3980×10^{-6}
	1.3447	0.2496	0.9517	9.1992×10^{-4}	57	0.77446	-0.03865	-0.39117	-0.23640	9.8871×10^{-6}
	1.4297	0.2164	0.6067	1.8130×10^{-4}	50	0.02977	-0.17769	0.76455	0.07083	9.3928×10^{-6}
	1.3781	0.1549	0.6753	7.2468×10^{-4}	52	-0.02694	-0.13399	0.95493	-0.01210	7.7835×10^{-6}

Table 10. Simulation results on the two coupled Hénon maps over 50 independent trials.

n	$\mathrm{PSO_{bif}}$				$\mathrm{PSO_{pp}}$		
	Mean F_{bif}	SD F_{bif}	Mean t_{end}	Suc[%]	Mean F_{pp}	SD F_{pp}	Suc[%]
4	5.00×10^{-4}	3.06×10^{-4}	74.3	100	8.32×10^{-6}	1.38×10^{-6}	100

$(\lambda_1, \lambda_2, \lambda_3)$ corresponding to the particle information of the $\mathrm{PSO_{bif}}$, and is defined by

$$\begin{aligned} F_{\mathrm{pp}}(\boldsymbol{z_p}) &= \left\| \boldsymbol{f}^n(\boldsymbol{x}_p, \boldsymbol{\lambda}) - \boldsymbol{x}_p \right\|, \\ &= \sqrt{\left(x_{1p+n} - x_{1p}\right)^2 + \left(y_{1p+n} - y_{1p}\right)^2 + \left(x_{2p+n} - x_{2p}\right)^2 + \left(y_{2p+n} - y_{2p}\right)^2}, \end{aligned} \tag{16}$$

where $\boldsymbol{z_p} \equiv (z_{p1}, z_{p2}, z_{p3}, z_{p4}) \equiv \boldsymbol{x}_p \equiv (x_{1p}, y_{1p}, x_{2p}, y_{2p})$, thus $N = 4$.

The experimental parameters of $\mathrm{PSO_{bif}}$ and $\mathrm{PSO_{pp}}$ are same as Table 1, except $M_{\mathrm{bif}} = M_{\mathrm{pp}} = 60$ and $T_{\max 1} = T_{\max 2} = 600$. The search ranges for the variables are summarized in Table 8.

Implementing the NLPSO, we detected the period doubling bifurcation points in the two coupled Hénon maps with $n = 4$-periodic points. The results of 10 simulations are summarized in Table 9. The proposed method effectively detected the bifurcation parameter $(\lambda_1, \lambda_2, \lambda_3)$ in all cases, and, all of the detected bifurcation points satisfied the criterion $F_{\mathrm{bif}} < 10^{-3}$ in fewer iterations than the maximum number of iterations $T_{\max 1} = 600$. The $\mathrm{PSO_{pp}}$ found 4-dimensional 4-periodic points to high accuracy without requiring careful initialization, gradient information or a Lyapunov exponent. Table 10 shows simulation results on the coupled Hénon maps over 50 independent trials. The success rates of both the $\mathrm{PSO_{bif}}$ and $\mathrm{PSO_{pp}}$ are 100%, and the mean t_{end} of the $\mathrm{PSO_{bif}}$ is only 74.3 iterations. In addition, the standard deviation values of two PSOs are low. Obviously, brute force cannot find the 3-dimensional bifurcation point from the same parameter space to a precision of 10^{-3} within 75 iterations.

5.4. *Accuracy level*

If the bifurcation point detected by the proposed method is assigned as the initial point of a bifurcation curve tracing, 10^{-3} should suffice for the accuracy of the $\mathrm{PSO_{bif}}$. On the other hand, it is important to investigate the behavior of the proposed method in the case of higher accuracy level. We ran 50 simulations using strict stop criterion 10^{-8} for both the $\mathrm{PSO_{bif}}$ and $\mathrm{PSO_{pp}}$, namely, $C_{\mathrm{bif}} = C_{\mathrm{pp}} = 10^{-8}$. Due to this change, on the circle and Hénon maps, the number of particles and the iteration limits of the $\mathrm{PSO_{bif}}$ were increased, namely $M_{\mathrm{bif}} = 50$ and $T_{\max 1} = 500$. Other experimental parameters were same as Table 1. On the coupled Hénon maps, the same parameters as Section 5.3 were used except $T_{\max 1} = 1500$.

Table 11. Simulation results on the circle map, the Hénon map and the coupled Hénon maps over 50 independent trials with strict stop criteria $C_{\rm bif} = C_{\rm pp} = 10^{-8}$.

	n	$\rm PSO_{bif}$				$\rm PSO_{pp}$		
		Mean $F_{\rm bif}$	SD $F_{\rm bif}$	Mean $t_{\rm end}$	Suc[%]	Mean $F_{\rm pp}$	SD $F_{\rm pp}$	Suc[%]
Circle	2	4.64×10^{-9}	3.05×10^{-9}	190.58	100	4.70×10^{-9}	3.12×10^{-9}	100
	3	4.93×10^{-9}	2.92×10^{-9}	238.22	100	4.69×10^{-9}	2.86×10^{-9}	100
	4	4.82×10^{-9}	2.98×10^{-9}	230.56	100	4.19×10^{-9}	3.00×10^{-9}	100
Hénon	5	4.98×10^{-9}	2.82×10^{-9}	211.84	100	6.35×10^{-9}	2.47×10^{-9}	100
	10	4.77×10^{-9}	3.21×10^{-9}	288.74	98	5.99×10^{-9}	2.70×10^{-9}	100
Coupled Hénon	4	5.11×10^{-9}	2.58×10^{-9}	415.30	100	8.25×10^{-9}	1.43×10^{-9}	100

The evaluation results are summarized in Table 11. The proposed method obtained 100% success rate for most of periodic points, and their mean $t_{\rm end}$ is below the iteration limit $T_{\rm max1} = 500$. On the Hénon map with $n = 10$, although the proposed method failed in the detection of the bifurcation point satisfying the accuracy 10^{-8}, the results are within the allowable range because it only failed one time, the mean $F_{\rm bif}$ satisfied the criterion, and the standard deviation value was low. This means that the proposed method can obtain period doubling bifurcation points with high accuracy and high robustness.

6. Comparison with Single PSO

To confirm an effectiveness of two PSOs with a nested structure, we applied a single PSO to the bifurcation point detection.

The algorithm of the single PSO for the bifurcation point detection is almost same as the PSO explained in Section 3. The particle position vector $\boldsymbol{z}$ corresponds to $(L + N)$ objective variables. The position vector of i-th particle is denoted by $\boldsymbol{z}_i = (z_{i1}, \cdots, z_{id}, \cdots, z_{iD})$, $(d = 1, 2, \cdots, D)$, where the first L components $\boldsymbol{z_b} = (z_{i1}, z_{i2}, \cdots, z_{iL})$ are the system parameter $\boldsymbol{\lambda}$ and the following N components $\boldsymbol{z_p} = (z_{i(L+1)}, z_{i(L+2)}, \cdots, z_{iD})$ serves as the periodic point $\boldsymbol{x}_p$. Thus, the PSO consists of $(L + N)$-dimensional particles $\boldsymbol{z} = (\boldsymbol{z_b}, \boldsymbol{z_p})$, namely, $D = L + N$.

An objective function F is defined by adding Eqs. (6) and (7) as

$$\begin{aligned} F(\boldsymbol{z}) &= F_{\rm bif}(\boldsymbol{z}) + F_{\rm pp}(\boldsymbol{z}), \\ &= \left|\det\left(D\boldsymbol{f}^n(\boldsymbol{z_p}, \boldsymbol{z_b}) + \boldsymbol{I}_N\right)\right| + \left\|\boldsymbol{f}^n(\boldsymbol{z_p}, \boldsymbol{z_b}) - \boldsymbol{z_p}\right\|, \end{aligned} \tag{17}$$

where $F_{\rm bif}(\boldsymbol{z}) = 0$ means that $\boldsymbol{z_b}$ produces a period doubling bifurcation at $\boldsymbol{z_p}$, and $F_{\rm pp}(\boldsymbol{z}) = 0$ means that $\boldsymbol{z_p}$ is n-periodic point on the map $\boldsymbol{f}$. Therefore, this is a minimization optimization with a minimum at 0. Updating of *gbest* $\boldsymbol{p}_g$ and *pbest* $\boldsymbol{p}_i$ of each particle i are carried out depending on the value of Eq. (17).

The termination condition is defined as

$$F(\boldsymbol{p}_g) < (C_{\rm bif} + C_{\rm pp}) \ \text{ OR } t > T_{\rm max}. \tag{18}$$

where $C_{\rm bif}$ and $C_{\rm pp}$ are the stop criterion on the bifurcation point and the periodic point, respectively.

We apply the single PSO to the circle map, the Hénon map and the coupled Hénon maps. The parameters for the simulation are summarized in Table 12. Please note that for a fair comparison, the number of particles and the maximum iterations were set as $(M_{\rm bif} \times M_{\rm pp})$ particles and $(T_{\rm max1} \times T_{\rm max2})$ iterations, which were used in the simulations of the NLPSO, respectively.

The results of 50 simulations are summarized in Table 13. We should note that there are some restriction conditions on the system parameters $\boldsymbol{z_b}$ and the periodic point $\boldsymbol{z_p}$. The system parameters $\boldsymbol{z_b}$ must be the parameter set for which n-periodic points exist, and the point $\boldsymbol{z_p}$ must be n-periodic point. Therefore, we evaluate the performance of the single PSO not only in terms of $F(\boldsymbol{p}_g)$ but also in $F_{\rm bif}(\boldsymbol{p}_g)$ and $F_{\rm pp}(\boldsymbol{p}_g)$. $F(\boldsymbol{p}_g)$, $F_{\rm bif}(\boldsymbol{p}_g)$ and $F_{\rm pp}(\boldsymbol{p}_g)$ were calculated by using the *gbest* $\boldsymbol{p}_g(t_{\rm end})$ when the independent simulation was ended. Suc. on NLPSO, $F_{\rm bif}(\boldsymbol{p}_g)$ and $F_{\rm pp}(\boldsymbol{p}_g)$ denote the success rate in achieving $F(\boldsymbol{p}_g) < (C_{\rm bif}+C_{\rm pp})$, $F_{\rm bif}(\boldsymbol{p}_g) < C_{\rm bif}$ and $F_{\rm pp}(\boldsymbol{p}_g) < C_{\rm pp}$, respectively. In all the maps, mean $F(\boldsymbol{p}_g)$ and $F_{\rm bif}(\boldsymbol{p}_g)$ satisfied the accuracy $(10^{-3} + 10^{-5})$ and 10^{-3}, respectively, and their success rates were almost 100%. However, in all

Table 12. Parameters of the single PSO.

	Circle	Hénon	Coupled Hénon
Number of dimensions $D(= L + N)$	$3(= 2 + 1)$	$4(= 2 + 2)$	$7(= 3 + 4)$
Stop criterion C_{bif}	1×10^{-3}	1×10^{-3}	1×10^{-3}
Stop criterion C_{pp}	1×10^{-5}	1×10^{-5}	1×10^{-5}
Maximum iterations $T_{\max}$	9×10^4	9×10^4	36×10^4
Number of particles M	900	900	3600
Inertia weight w		0.729	
Acceleration coefficients c_1, c_2		1.494	

Table 13. Simulation results of the single PSO over 50 independent trials.

	n	Mean $F(\boldsymbol{p}_g)$	Mean t_{end}	Suc. of $F(\boldsymbol{p}_g)$	Mean $F_{\mathrm{bif}}(\boldsymbol{p}_g)$	Suc. of $F_{\mathrm{bif}}(\boldsymbol{p}_g)$	Mean $F_{\mathrm{pp}}(\boldsymbol{p}_g)$	Suc. of $F_{\mathrm{pp}}(\boldsymbol{p}_g)$
Circle	2	6.18×10^{-4}	23.1	100%	3.27×10^{-4}	100%	2.91×10^{-4}	4%
	3	7.00×10^{-4}	46.2	100%	3.89×10^{-4}	100%	3.11×10^{-4}	2%
	4	6.85×10^{-4}	42.6	100%	2.93×10^{-4}	100%	3.91×10^{-4}	0%
Hénon	5	7.66×10^{-4}	117.1	100%	1.96×10^{-4}	100%	5.70×10^{-4}	0%
	10	7.66×10^{-4}	415.1	100%	1.99×10^{-4}	100%	5.99×10^{-4}	0%
Coupled Hénon	2	1.45×10^{-4}	34174.7	94%	1.11×10^{-4}	100%	1.34×10^{-3}	0%

the maps, mean $F(\boldsymbol{p}_g)$ did not satisfy the accuracy 10^{-5}, and the success rates were almost 0%. This means that the found periodic point did not satisfy the accuracy 10^{-5}, thus the found bifurcation parameter was not correct, but false even though its F_{bif} satisfied the criterion. If C_{bif} and C_{pp} are more strict such as 10^{-8}, it is clear that it is harder for the single PSO to find the correct bifurcation parameters. Furthermore, the mean t_{end} is larger than the results of the NLPSO. These results show that the single PSO cannot find correct periodic bifurcation parameters satisfying the restriction conditions on high-periodic point and high-dimensional map with many system parameters, and the nested structure is fit to easily find the bifurcation parameters.

7. Conclusions

This paper has proposed a period doubling bifurcation detection strategy with two PSOs; $\mathrm{PSO}_{\mathrm{bif}}$, which searches for the period doubling bifurcation parameter, and $\mathrm{PSO}_{\mathrm{pp}}$, which searches for the periodic point depending on the system parameters corresponding to the particle information of $\mathrm{PSO}_{\mathrm{bif}}$. In the proposed method, called NLPSO, the $\mathrm{PSO}_{\mathrm{pp}}$ nests within the $\mathrm{PSO}_{\mathrm{bif}}$. Although the problem contains two interdependent objective functions, these functions are not simultaneously solved by the proposed NLPSO, so one bifurcation point is detected among multiple solutions.

Using the proposed method, we directly detected period doubling bifurcations of various periodic points, including high-periodic points, in the circle, Hénon and coupled Hénon maps. The proposed method accurately detected the period doubling bifurcation parameters of all periodic points in all of the constructed maps, regardless of the stability of the periodic points. Obviously, brute force cannot find the bifurcation point from the same parameter space to a precision of 10^{-3} within 300 iterations. This suggests the applicability of the proposed method to high-dimensional periodic points in high-dimensional maps with large parameters spaces. By assigning the bifurcation point detected by the proposed method as the initial point of a bifurcation curve tracing, we could solve the initial value problems of conventional bifurcation analyses. We emphasize that the proposed method detects periodic and bifurcation points without requiring the second-order differential of the map or carefully set initial values, which are essential in gradient-based algorithms such as the Newton–Raphson method. The initial values of the two PSOs in the proposed method need only be randomly seeded in the search space. By simply changing the parameter of the periodic number, we can detect the bifurcation points of various periodic points in the same map without changing the algorithms or the objective functions. From these features, we conclude that the pro-

posed method effectively detects period doubling bifurcation points with high accuracy, high robustness, versatile usability and rapid convergence speed.

In future work, we will apply the proposed method to other bifurcations such as saddle-node and Neimark–Sacker bifurcations. Because our present method cannot detect saddle-node bifurcation points, refinement is essential. We are also interested in unique bifurcations in composite dynamical systems, such as grazing bifurcations and border collision bifurcations. Furthermore, the proposed method should be applied to continuous dynamical systems and noisy systems, and to the detection of bifurcation curves as well as bifurcation points. The relationship between the simulation results and the PSO parameters (such as number of particles and maximum number of iterations) should also be investigated. Moreover, we will modify and improve the algorithm of the proposed method. In this study, we have used the fully-connected PSO where *gbest* with the best objective function value among all particles is used in the update equation since this type of PSO is the simplest and includes only a fraction of parameters. However, other type of PSO such as PSO with neighborhood topology and population-based optimizers other than the PSO should be tried. In addition, we hope to extend NLPSO beyond bifurcation analysis and into circuit design, chaos control and other applications.

Acknowledgments

This work was supported by JSPS KAKENHI Grant Number 16K16124.

References

Barrera, J., Flores, J. J. & Fuerte-Esquivel, C. [2008] "Generating complete bifurcation diagrams using a dynamic environment particle swarm optimization algorithm," *Journal of Artificial Evolution and Applications* **2008**, 7.

Doedel, E. J. & Oldeman, B. E. [2012] http://indy.cs.concordia.ca/auto/.

ERATO, JST [2004] http://bunki.ait.tokushima-u.ac.jp:50080/.

Gallas, J. A. [1993] "Structure of the parameter space of the hénon map," *Physical Review Letters* **70**, 2714.

Gao, F., Gao, H., Li, Z., Tong, H. & Lee, J. [2009] "Detecting unstable periodic orbits of nonlinear mappings by a novel quantum-behaved particle swarm optimization non-lyapunov way," *Chaos, Solitons & Fractals* **42**, 2450–2463.

Hénon, M. [1976] "A two-dimensional mapping with a strange attractor," *Comm. Math. Phys.* **50**, 69–77.

Kawakami, H. [1984] "Bifurcation of periodic responses in forced dynamic nonlinear circuits: Computation of bifurcation values of the system parameters," *IEEE Trans. on Circuits and Systems* **31**, 248–260.

Kennedy, J. & Eberhart, R. [1995] "Particle swarm optimization," *Proc. of IEEE Int. Joint Conf. on Neural Netw.*, pp. 1942–1948.

Kousaka, T., Ueta, T. & Kawakami, H. [1999] "Bifurcation of switched nonlinear dynamical systems," *IEEE Trans. on Circuits and Systems II* **2**, 1451–1458.

Liu, B., Wang, L., Jin, Y., Tang, F. & Huang, D. [2006] "Detecting orbits of chaotic systems by particle swarm optimization," *Chaos, Solitons & Fractals* **29**, 454–461.

Matsushita, H. & Saito, T. [2011] "Application of particle swarm optimization to parameter search in dynamical systems," *Nonlinear Theory and Its Applications, IEICE* **2**, 458–471.

Parsopoulos, K. & Vrahatis, M. [2003] "Computing periodic orbits of nondifferentiable/discontinuous mappings through particle swarm optimization," *Proc. of IEEE 2003 Swarm Intelligence Symposium*, pp. 34–41.

Petalas, Y. G., Parsopoulos, K. E. & Vrahatis, M. N. [2008] "Stochastic optimization for detecting periodic orbits of nonlinear mappings," *Nonlinear Phenomena in Complex Systems* **11**, 285–291.

Sausedo-Solorio, J. M. & Pisarchik, A. N. [2011] "Dynamics of unidirectionally coupled bistable hénon maps," *Physics Letters A* **375**, 3677–3681.

Shi, Y. & Eberhart, R. [1998] "A modified particle swarm optimizers," *Proc. of IEEE Int. Conf. on Computational Intelligence*, pp. 69–73.

Skokos, C., Parsopoulos, K. E., Patsis, P. A. & Vrahatis, M. N. [2005] "Particle swarm optimization: an efficient method for tracing periodic orbits in three-dimensional galactic potentials," *Monthly Notices of the Royal Astronomical Society* **359**, 251–260.

Trelea, I. C. [2003] "The particle swarm optimization algorithm: convergence analysis and parameter selection," *Information Processing Letters* **85**, 317–325.

Ueta, T., Tsueike, M., Kawakami, H., Toshinaga, T. & Katsura, Y. [1997] "A computation of bifurcation parameter values for limit cycles," *IEICE Trans. on on Fundamentals of Electronics, Communications and Computer Sciences* **E80**, 1725–1728.